

Multifunctional nanocarriers for mammographic quantification of tumor dosing and prognosis of breast cancer therapy

Efstathios Karathanasis^a, Leslie Chan^a, Sri R. Balusu^a, Carl J. D'Orsi^b, Ananth V. Annapragada^c, Ioannis Sechopoulos^b, Ravi V. Bellamkonda^{a,*}

^aWallace H. Coulter Department of Biomedical Engineering, Georgia Institute of Technology and Emory University, Atlanta, GA 30332, USA

^bDepartment of Radiology and Winship Cancer Institute, Emory University School of Medicine, Atlanta, GA 30322, USA

^cSchool of Health Information Sciences, University of Texas Health Science Center, 7000 Fannin Street, Houston, TX 77030, USA

ARTICLE INFO

Article history:

Received 5 August 2008

Accepted 22 August 2008

Available online 23 September 2008

Keywords:

Multifunctional nanoparticle

Personalized medicine

Iodine-doxorubicin-loaded liposome

Breast cancer imaging

Prediction of chemotherapy

ABSTRACT

Nanoscale therapeutic interventions are increasingly important elements in the portfolio of cancer therapeutics. The efficacy of nanotherapeutics is dictated, in part, by the access they have to tumors via the leaky tumor vasculature. Yet, the extent of tumor vessel leakiness in individual tumors varies widely resulting in a correspondingly wide tumor dosing and resulting range of responses to therapy. Here we report the design of a multifunctional nanocarrier that simultaneously encapsulates a chemotherapeutic and a contrast agent which enables a personalized nanotherapeutic approach for breast cancer therapy by permitting tracking of the nanocarrier distribution by mammography, a widely used imaging modality. Following systemic administration in a rat breast tumor model, imaging demonstrated a wide range of intratumoral deposition of the nanocarriers, indicating variable tumor vessel leakiness. Notably, specific tumors that exhibited high uptake of the nanocarrier as visualized by imaging were precisely the animals that responded best to the treatment as quantified by low tumor growth and prolonged survival.

© 2008 Elsevier Ltd. All rights reserved.

1. Introduction

Nanocarriers [1,2] are excellent delivery vehicles for chemotherapeutic drugs, increasing delivery efficiency to the targeted tumor while reducing off-target delivery, thus increasing the overall therapeutic index [3]. For instance, liposomal anthracyclines [4] and nanoparticle albumin-bound paclitaxel [1] are examples of nanotherapeutics approved for clinical use. Furthermore, nanoscale control in fabrication allows for multifunctional carriers [5–7] that can (i) carry large payloads of therapeutic drugs or diagnostic imaging/contrast agents [8,9]; (ii) modulate pharmacokinetics and biodistribution when systemically administered to increase accumulation in tumor site, and (iii) enable presentation of targeting ligands to increase target tumor affinity and selectivity [10,11]. Here we demonstrate that incorporating a contrast agent along with anti-cancer therapeutic can potentially enable personalized cancer therapy that facilitates diagnosing, treating and monitoring of individual cancer treatment efficacy by a clinically relevant, breast cancer imaging modality, mammography [7,12–15].

The success of systemically delivered nanotherapeutics for solid tumors is critically dependent on the access that these agents have to tumors via the so-called tumor leaky vasculature. The tumor's complex microvasculature network [16] consists of immature blood microvessels with hypervascularization, abnormal vascular architecture, increased leakage through the vessel wall and lack of lymphatic drainage [17]. Nanoscale particles preferentially accumulate in solid tumors by passive convective transport through leaky endothelium (a process termed *extravasation*) [18–20]. Unlike small molecules, since the convective transport of these particles far outweighs the diffusive component, they do not return to the blood stream. To date however, no clinical tools exist to non-invasively determine whether the tumor blood vessels of an individual patient are permeable to a nanotherapeutic or not. For instance, the current clinical protocols for liposomal chemotherapy consist of a standard dose every 3–4 weeks [21]. No prior knowledge of tumor vessel status, especially leakiness, is taken into account for dose scheduling. However, it is well-known that the degree of tumor vasculature leakiness differs among same type tumors [22–24]. One recent example demonstrating the critical role that tumor vasculature plays in determining therapeutic outcomes comes from the work of Jain [25,26], where it was shown that the restructuring of tumor vasculature (a process termed 'normalization') leads to better chemotherapeutic outcomes. While antiangiogenic therapies focus on destroying tumor-related blood vessels

* Corresponding author. Wallace H. Coulter Department of Biomedical Engineering, Georgia Institute of Technology/Emory University, 3108 UA Whitaker Building, 313 Ferst Drive, Atlanta, GA 30332, USA. Tel.: +1 404 385 5038; fax: +1 404 385 5044.

E-mail address: ravi@gatech.edu (R.V. Bellamkonda).

compromising the efficiency of subsequent chemotherapy, optimal scheduling and dosing of these therapies can ‘normalize’ the abnormal tumor vasculature for better delivery of oxygen (eliminating hypoxia and its complications) and other drugs.

To address the need for non-invasive tracking of nanoscale chemotherapeutic dosing to individual tumors, a multifunctional liposomal nanocarrier was developed co-encapsulating an X-ray contrast agent (iodixanol) for imaging and a chemotherapeutic (doxorubicin) for treatment. In this work, the nanocarrier’s extravasation in a rat breast tumor model was non-invasively quantified by mammographic imaging and used to predict the efficacy of the therapy as monitored by tumor growth and survival rates.

2. Methods

2.1. Fabrication of the multifunctional nanocarrier

A highly concentrated iodine solution (550 mg/mL iodine) was prepared by dissolving iodixanol powder (lyophilized from Visipaque 320, GE Healthcare, Milwaukee, WI) in a 250 mM ammonium sulfate solution under stirring and heating at 70 °C. The phospholipids 1,2-dipalmitoyl-*sn*-glycero-3-phosphocholine (DPPC) and 1,2 distearyl-*sn*-glycero-phosphoethanolamine poly(ethylene glycol)₂₀₀₀ (DSPE-PEG₂₀₀₀) were used as the lipid matrix for the liposomes (Genzyme Pharmaceuticals, Cambridge, MA). A lipid composition of DPPC, cholesterol and DSPE-PEG₂₀₀₀ in the molar ratio of 55:40:5 was used. The lipids were dissolved in ethanol and hydrated with the iodine solution at 70 °C followed by sequential extrusion in a Lipex Biomembranes Extruder (Northern Lipids, Vancouver, Canada), to size the liposomes to 100 nm. Free, unencapsulated ammonium sulfate (and iodixanol) was replaced by a saline solution (400 mM NaCl at pH ~ 7) using a 1-day dialysis with a 100 kDa MWCO dialysis tubing to establish an ammonium sulfate gradient for remote loading of doxorubicin (DXR). Briefly, liposomes and DXR were mixed at a ratio of 0.1 mg DXR per 1 mg of DPPC in the liposomes. The liposome–DXR suspension was heated at 35 °C for 25 min. The liposomes were then left overnight at room temperature and then dialyzed twice in 100 kDa MWCO membrane against 400 mM NaCl to remove unencapsulated DXR. Following concentration via diafiltration using MicroKros modules (Spectrum Laboratories, California) with a 50 nm cutoff pore size, the size of the liposomes was determined by dynamic light scattering (90 Plus Particle Size Analyzer, Brookhaven Instruments, Holtsville, NY). Prior to administration, the final iodine and DXR levels were quantified through spectrophotometry at 245 and 480 nm, respectively.

2.2. Mammary adenocarcinoma cell culture

The 13762 MAT B III cells (American Type Culture Collection), a rat mammary adenocarcinoma cell line, was maintained in McCoy’s 5A medium supplemented with 10% fetal bovine serum and 1% penicillin–streptomycin under conditions of 5% CO₂ and 95% humidity at 37 °C.

2.3. In vitro cytotoxicity experiment

Cytotoxicity studies were performed by seeding the 13762 MAT BIII cells at a density of 10⁵ cells/well in 6-well plate 24 h before incubation with the formulations. Prior to incubation, cells were washed three times with fresh medium and then incubated with the treatment for 180 min at a concentration of 150 μM doxorubicin per well. The treatments consisted of doxorubicin, doxorubicin loaded liposomes, doxorubicin/iodine co-loaded liposomes, and blank liposomes. Doxorubicin loaded liposomes were prepared following established methods [27]. After treatment application, the cells were washed three times with fresh medium and then incubated for 48 h at 37 °C and 5% CO₂ in a humidified environment. The number of viable cells was determined using a formazan-based cell counting assay (CCK-8). Untreated cells served as live controls for normalization of the data.

2.4. Animal model

All animal procedures were approved by the Institutional Animal Care and Use Committee (IACUC) of Georgia Institute of Technology. For the tumor model, the 13762 MAT B III cell line was used. Before inoculation, the cells were grown in 90% McCoy’s 5A medium and 10% fetal bovine serum. A 0.2 mL aliquot containing 10⁶ cancer cells was subcutaneously injected into the right flank of female Fisher rats with ages of 8–9 weeks (Harlan, Indianapolis, IN). Caliper measurements were used to estimate tumor size and the tumor volume was calculated as: $V_{\text{tumor}} = (d_1^2 \times d_2)/2$, where d_1 and d_2 are the minimum and maximum diameters.

2.5. X-ray imaging and treatment

Once the appropriate tumor sizes were established (day 7 after tumor inoculation, volume ~ 500 mm³), the animals were used in the imaging studies. The

animals were imaged using a clinical digital mammography system (Senographe 2000D, GE Healthcare, Milwaukee, WI). To maximize the number of photons with energies above the K-edge of iodine (approx. 33.2 keV) [28], the imaging studies were performed with a 49 kVp, 63 mAs X-ray spectrum, using a rhodium target and a 25 μm thick rhodium filter with an added 0.254 mm thick copper filter. The resultant X-ray spectrum was estimated using the XSPECT simulation program developed at Henry Ford Health Systems (Detroit, MI) based on semi-empirical models. To compute the radiation dose to the animals during X-ray imaging, a previously validated Monte Carlo simulation for dosimetry studies [29] was modified to include a simplified version of the animal geometry. In the simulation, the animals were represented as a cylinder of water with a length of 10 cm and a diameter of 4 cm. To estimate the dose to the cylinder from the X-ray spectrum used in the imaging studies, the Monte Carlo simulation was performed repeatedly with monochromatic X-rays with energies from 20 keV to 49 keV in 0.5 keV steps. To achieve the necessary statistical accuracy, one million photons per energy level were simulated. The monochromatic results were combined with the X-ray spectrum obtained with the XSPECT simulation program using the method described by Boone [30].

At day 7 after tumor inoculation, a group of animals ($n = 8$) was imaged before ($t = 0$) and at defined time points after IV injection ($t = 2$ and 30 min, 24 h, 72 h) of the nanocarrier. A control group of animals ($n = 8$) was imaged at the same time points upon injection of 0.5 mL of saline. The tumor growth of each animal was monitored every day using caliper measurements. In the end of the study, the animals were euthanized using a CO₂ chamber.

2.6. Intratumoral levels of doxorubicin

A different group of animals ($n = 8$) was imaged before ($t = 0$) and at defined time points after IV injection ($t = 24$ h and 72 h) of the nanocarrier. Immediately after the last imaging session, animals were anesthetized with an intraperitoneal injection of 50 and 10 mg/kg of ketamine and xylazine respectively and transcardially perfused with heparinized (1 unit/mL) phosphate buffered saline (PBS). The tumors were retrieved, washed with PBS and blotted dry. Tumors were weighed and DXR was extracted following methods described elsewhere [31]. Briefly, the tumors were homogenized in distilled, deionized water (20% wt/vol) using a Polytron Homogenizer (Brinkmann Instruments, Westbury, NY). Homogenates (200 μL) were mixed with 100 μL of 10% Triton X-100, 200 μL of water and 1500 μL of acidified isopropanol (0.75 N HCl). Mixtures were stored overnight at –20 °C to extract the drug and then warmed at room temperature and vortexed for 5 min. The samples were then centrifuged at 15 000 g for 20 min. Fluorescence of supernatants was analyzed to determine DXR content ($\lambda_{\text{ex}} = 485$, $\lambda_{\text{em}} = 590$). Tumor samples from an animal treated with a saline injection were used to correct for background fluorescence.

2.7. Survival study

At day 7 after tumor inoculation, a different group of animals ($n = 8$) was imaged before and after administration ($t = 2$ min, 24 h, 72 h) of the nanocarrier using the mammography system. At day 14 after tumor inoculation, the animals were injected again with the same dose of the nanocarrier and imaged at the same time points. Tumor growth was allowed to progress until the animal showed signs of morbidity, at which point, the animals were euthanized using a CO₂ chamber. Time of death was determined to be the following day. The survival time of a control group ($n = 10$) was also determined.

2.8. Image analysis

The sequential image acquisitions provided the dynamics of the nanocarrier’s intratumoral accumulation over time. The grey levels in raw data (DICOM format) were measured using ImageJ software (NIH, Bethesda, MD). An ellipsoid region of interest was used for the measurements surrounding the entire tumor lesion. Since mammography is not a tomographic but a summation procedure, the observed tumor enhancement represents the summation of the absolute enhancement due to the contrast agent and the enhancement of overlying tissue structures. To normalize with respect to the overlying tissues, we computed a relative enhancement by subtracting the pre-contrast enhancement value from the post-contrast enhancement value.

For display purposes only, the histograms of the radiographic images were matched using ImageJ. The quality of these images was improved by sharpening the images using the ‘unsharp mask’ function in ImageJ. This simple sharpening operator enhances edges and other high frequency components in an image by subtracting a blurred copy of the image (created by Gaussian blurring) and rescaling the image to obtain the same contrast of large (low-frequency) structures as in the input image [32]. The mask weight (intensity of sharpening) was set at 0.7 and the Gaussian blur had a radius of 15 pixels. This processing was performed for display of the images only whereas quantitative analysis was performed with the original, unprocessed images.

2.9. Data and statistical analysis

To determine the significance of the grey levels variation, tumor volumes, and survival times between the treated and the control group at different time points, an unpaired two-tailed Student *t*-test analysis was performed (SPSS 15, Chicago, IL). A *p*-value less than 0.05 was used to confirm significant differences at the 95% confidence level. The tumor signal enhancement profiles and tumor growth curves were fitted into an exponential function [33] using nonlinear regression (Levenberg–Marquardt algorithm) to compute the enhancement rate constant ($K^{\text{enhancement}}$) and the tumor growth rate constant ($K^{\text{tumor growth}}$), respectively. The area under the curve of signal enhancement profiles ($\text{AUC}^{\text{enhancement}}$) was estimated using the Gauss-Legendre orthogonal polynomial approximation. The correlation between the signal enhancement and the tumor growth rate, or survival rate or intratumoral drug content was determined using Pearson's correlation. The correctness of the model was determined by examining the residuals plots and other statistical tests.

3. Results

3.1. Characterization of the nanocarrier

The nanocarriers encapsulated 110 mg/mL of iodine and 2.8 mg/mL of doxorubicin (DXR) respectively. The average diameter of the nanocarrier was 102 nm (SD = 12), a size known to prevent renal clearance and facilitate clearance via the liver [4]. An *in vitro* leakage experiment against isotonic phosphate buffered saline exhibited low leakage of the encapsulated iodine and doxorubicin (less than 5% and 1% of the initial payload respectively) at room temperature over a period of 3 days.

3.2. *In vitro* cytotoxicity study

To determine the nanocarrier's antitumor potency, its cytotoxic effect on mammary adenocarcinoma cells (13762 MAT BIII) was compared to doxorubicin (free or liposomal). As shown in Fig. 1, cells exposed to blank or iodine-loaded liposomes remained unaffected and exhibited approximately 100% viability. Free doxorubicin and DXR-loaded liposomes demonstrated a significant increase in cytotoxicity exhibited by a dramatic reduction in cell viability. The liposomal nanocarrier co-loaded with iodine and DXR displayed similar cytotoxicity to the conventional, non-iodine containing DXR-loaded liposomes indicating non-interference of DXR function due to the presence of iodine contrast agent.

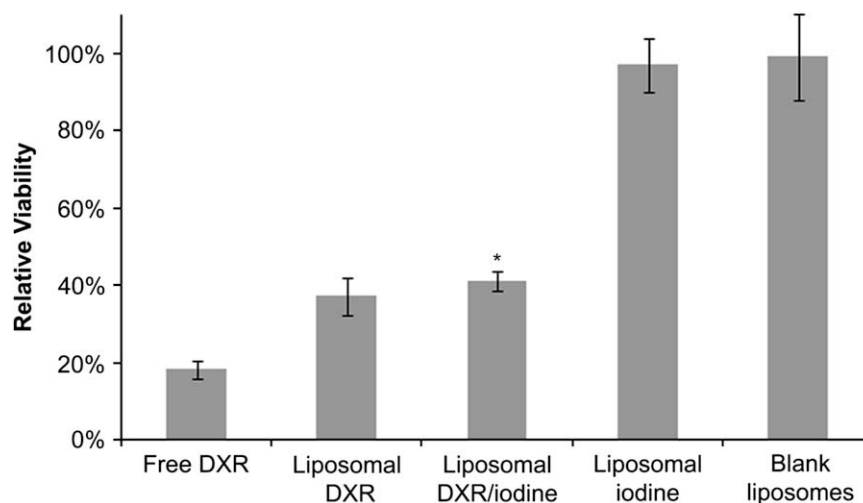


Fig. 1. Cytotoxicity of the nanocarrier co-encapsulating iodine and DXR on 13762 mammary adenocarcinoma cells. Blank and iodine-loaded liposomes (negative control) had no cytotoxic effect on the tumor cells showing an almost 100% viability. The co-loaded liposomal nanocarrier exhibited significant cytotoxic potency (41% viable cells) when compared to the negative controls and similar potency when compared to conventional DXR-loaded liposomes. As expected free DXR displayed high cytotoxicity. Data points represent group mean \pm s.d. Data points marked with asterisks are statistically significant relative to control treated with blank liposomes (* $P < 0.009$; *t*-test, two-tailed).

3.3. Imaging using a clinical mammography system

Initial imaging studies were performed to determine the dose of the nanocarrier required for detection and quantification of extravasation of the agent into tumors. The nanocarrier was tested in adult female rats using a breast tumor model developed by inoculation of 13762 MAT BIII cells into the right flank of rats. Under the operating conditions of the mammography unit, the animal received a radiation dose of 0.39 mGy per imaging session (compared to about 2 mGy radiation dose of a standard single-view clinical mammogram). In pilot imaging sessions (data not shown) where animals were injected intravascularly with different doses of the agent, the threshold for visualization of blood vessels was identified to be about 12 mg/mL iodine in the blood which corresponds to a dose of 780 mg iodine per kg body weight (mg/kg bw). To eliminate signal from the blood vessels and probe the nanocarrier's extravasation into tumor, contrast-enhanced imaging was performed with IV injection of the nanocarrier at a dose of 390 mg/kg bw iodine which produced a concentration of ~ 6 mg/mL iodine in blood, a concentration below the threshold for detection of iodine in the blood. This allowed detection of the extravasated nanocarrier as early as 24 h post-injection, with no interference from the vascular signal. The volume of injection was 3.5 mL/kg bw corresponding to a dose of 10 mg/kg bw doxorubicin. Fig. 2 shows the pre-injection ($t = 0$) and post-injection images ($t = 24$ and 72 h). In the 24-h image no blood vessels were visible in the normal tissue while the spleen and the tumor were enhanced. Spleen enhancement is consistent with clearance of liposomes via the Reticulo Endothelial System (RES).

3.4. Correlation of treatment efficacy to dosing determined by mammography

When tumors were monitored for 3 days post-injection, it was observed that the X-ray absorption in tumors due to extravasated nanocarrier varied widely both spatially and temporally, suggesting that each tumor had different tumor vessel leakiness. Fig. 3a summarizes the 3-day time course of the tumor enhancement of each animal injected with the nanocarrier. The grey levels of each tumor was quantified and a relative enhancement was calculated by normalizing each post-injection value ($t > 0$) with respect to its pre-injection value ($t = 0$). The enhancement profiles exhibit

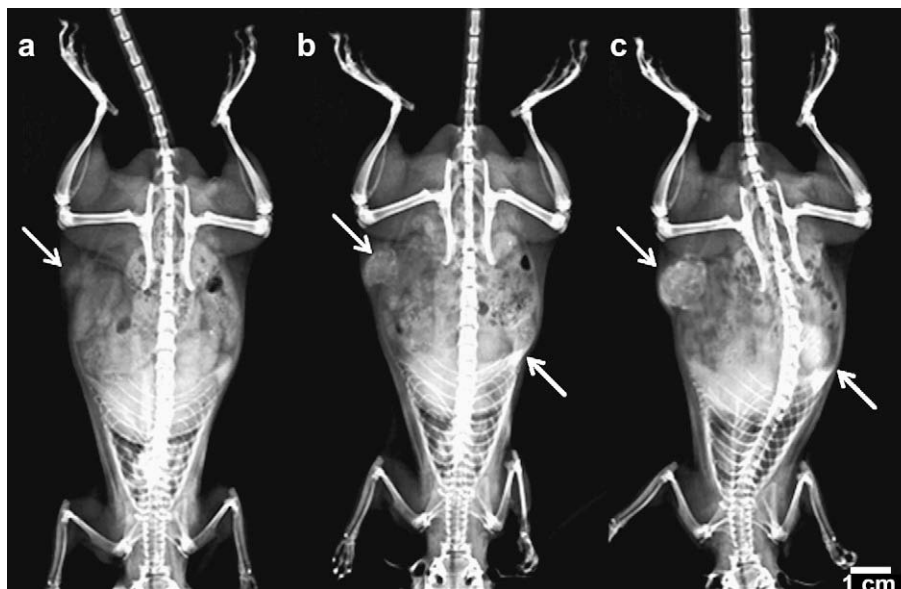


Fig. 2. Whole body X-ray images of a rat breast tumor using a clinical digital mammography system. (a) before and (b) 24 h and (c) 72 h after administration of the nanocarrier at a dose of 390 mg iodine per kg body weight showing the 3-day intratumoral deposition of the agent. The signal enhancement in the tumor (upper arrows) and spleen (lower arrows) is clearly visible in the post-injection images.

dissimilar patterns in different animals/tumors. During the 3-day time course, some tumors exhibited a rapid and significant increase of the enhancement (e.g. animals 1 and 2 in Fig. 3a) whereas other tumors showed a slow and low increase (e.g. animals 7 and 8 in Fig. 3a). The pattern of tumor enhancement of the entire group is plotted in Fig. 3b and compared against the normal tissue of the same animals (soft tissue of the leg was used for measurement of the signal from normal tissue). While the tumor displays a significant enhancement, no enhancement was observed in normal tissues suggesting that the nanocarrier levels in the blood were below the detectable threshold by mammography. In contrast, tumors within a control group of rats ($n = 6$) not given a contrast agent remained unenhanced implying that no endogenous changes of the tumor tissue contributed to the enhancement.

Tumor response to the doxorubicin load of the nanocarrier was evaluated by quantitatively following the tumor size for several days after injection. Fig. 3c compares the tumor growth rate of the treated group and a control group injected only with saline. The nanocarrier injection slowed the progress of the tumor, displaying statistically significant effectiveness 5 days post-injection. Importantly, a significant correlation between the imaging measurements and the response to treatment was observed. Fig. 3d shows the tumor growth rate of each individual treated animal and the control group. Higher uptake of the nanocarrier by the tumor as imaged with mammography indicating leakier vasculature correlated to a slower tumor growth rate and a better therapeutic outcome. To better characterize the imaging-enabled prediction accuracy, we calculated the tumor growth rate constant ($K^{\text{tumor growth}}$) and signal enhancement rate constant ($K^{\text{enhancement}}$) of each animal, representing a measure of the tumor response to treatment and the prognostic assessment by imaging, respectively. Fig. 3e demonstrates a strong correlation between $K^{\text{tumor growth}}$ and $K^{\text{enhancement}}$ with the less leaky tumors (low $K^{\text{enhancement}}$) having faster tumor progress (high $K^{\text{tumor growth}}$) and vice versa.

The agreement of the imaging-based prediction to the anti-tumor effect in terms of tumor growth rate suggests that high levels of drug deposited in tumors that displayed high signal enhancement in imaging. To further investigate the levels of intratumoral, extravascular deposition of the agent and its correlation to the

imaging data, a different group of animal was imaged (at 24 and 72 h after injection), euthanized immediately after the last imaging session, and the tumors were extracted and analyzed for DXR content. As shown in Fig. 3f, the area under the curve of the signal enhancement profile ($AUC^{\text{enhancement}}$) of each animal, a measure of the intratumoral levels of the iodinated contrast agent load of the agent, and the intratumoral levels of the drug strongly correlated.

3.5. Survival study

The clinical protocol for 100 nm scale liposomal doxorubicin therapy involves multiple injections spread over weeks. Therefore, in a subsequent study, a group of animals was injected with the multifunctional Iodixanol/DXR co-encapsulated nanocarriers once a week for a total of two weeks to determine whether a mammography-based prognostic assessment of each treatment cycle enables a reliable prediction of the outcome of the entire treatment. The animals were imaged before ($t = 0$) and after ($t = 24$ and 72 h) each injection and tumor signal enhancement was quantified by mammography in a similar fashion as before. An enhancement rate constant $K^{\text{enhancement}}$ was determined for each cycle ($k1$ and $k2$; Fig. 4a) representing both tumor dosing and a prognostic assessment for each treatment cycle. While some tumors exhibited similar $k1$ and $k2$ (e.g. rats 4 and 5 in Fig. 4a), other tumors displayed high $k1$ and low $k2$ (e.g. rats 3 and 8) and vice versa (e.g. rat 6). This is not surprising as aggressive tumor models are known to display a vasculature with continuous spatial and temporal changes during growth, regression, and relapse [22] and chemotherapy may not affect $k1/k2$ on the time scales of this experiment. The therapeutic effect of the nanocarrier was determined by comparing the survival times of treated animals to untreated animals (Fig. 4b). A statistically significant increase in survival time of the treated animals (24.1 ± 3.8 days; expressed as mean \pm s.d.) was observed when compared to the control group (13.3 ± 1.5 days), an increase of mean survival time of $\sim 80\%$. While the treatment substantially prolonged the survival of few animals to 28–30 days, most of the treated group survived 21–22 days indicating that the two-cycle application of the nanocarrier had variable antitumor effect among the animals. To realize the relation of the imaging-enabled prediction to the antitumor effect of the

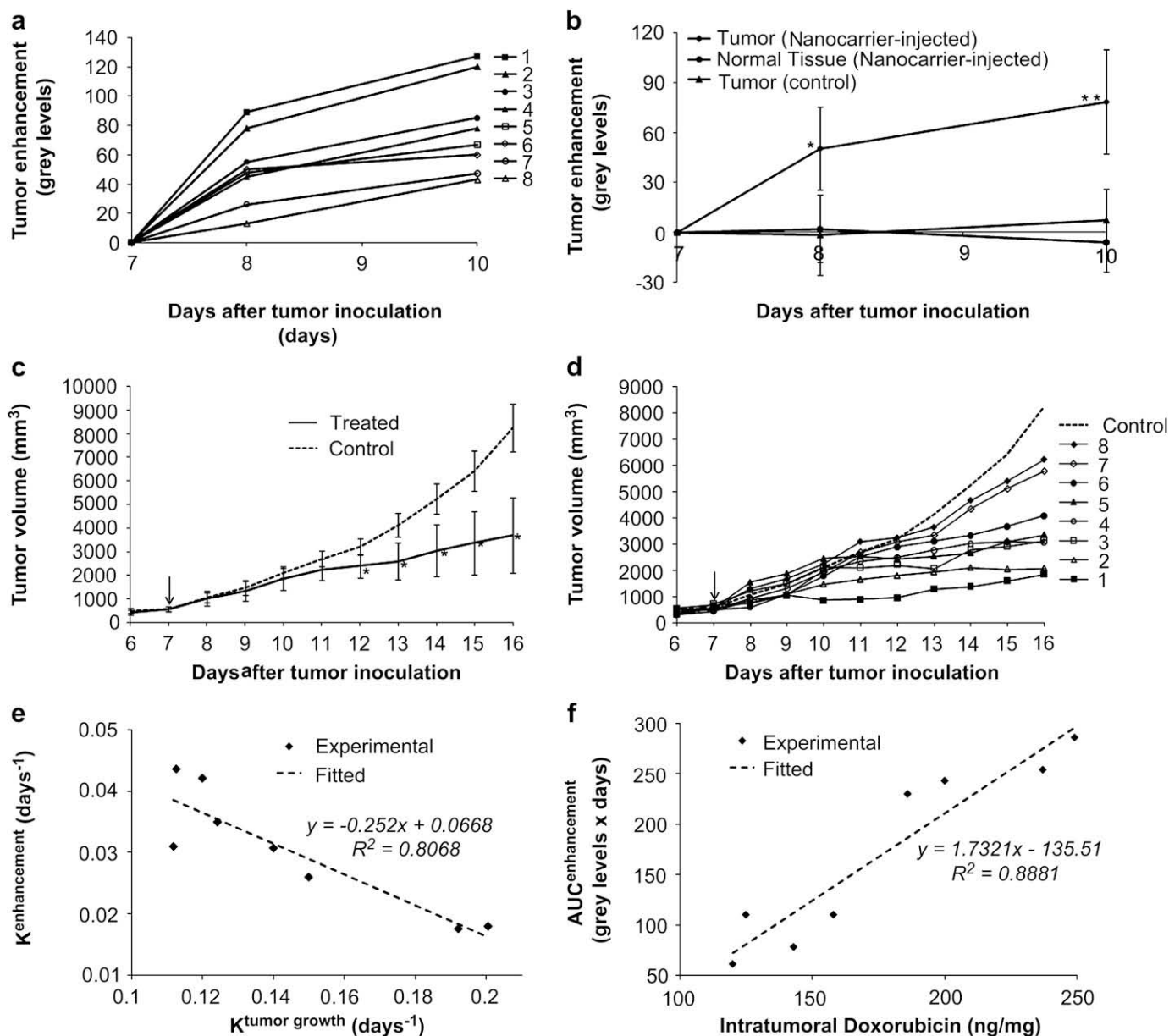


Fig. 3. Comparison of the tumor signal enhancement as imaged with mammography to tumor growth rates and intratumoral drug levels. (a) The 3-day pattern of the tumor signal enhancement of each animal following injection of the nanocarrier (390 mg/kg bw iodine) to a group of rats ($n=8$) indicates a high variability of the tumors' leakiness; (b) The tumor enhancement due to the nanocarrier was higher than that of normal tissue which showed no substantial enhancement. Without administration of the nanocarrier, the tumor lesion of a control group of animals injected with saline ($n=6$) showed no enhancement. Data points represent group mean \pm s.d. Data points marked with asterisks are statistically significant relative to control tumor injected with no contrast agent (* $P < 0.0005$, ** $P < 0.00002$; t -test, two-tailed); (c) Administration of the nanocarrier to the treated group ($n=8$) at day 7 (arrow) significantly decreased the tumor growth rate when compared to an untreated group ($n=12$). Data points represent group mean \pm s.d. Data points marked with asterisks are statistically significant relative to control tumor injected with saline (* $P < 0.01$; t -test, two-tailed); (d) The tumor of each animal of the treated group responded differently to the nanocarrier treatment as indicated by the variable tumor growth curves; (e) The tumor response to the treatment represented by the tumor growth rate constant ($K^{\text{tumor growth}}$) was strongly correlated to the imaging-based prognostic assessment represented by the tumor signal enhancement rate constant $K^{\text{enhancement}}$ ($P < 0.002$; t -test, single-tailed); (f) The $K^{\text{enhancement}}$ of a group of animals ($n=8$) injected with the nanoprobe strongly correlated to the intratumoral amounts of drug directly measured post-mortem ($p < 0.00001$; t -test, single-tailed).

entire treatment, the overall signal enhancement rate constant ($K=k_1+k_2$) obtained from imaging was plotted against the survival time of each individual animal in Fig. 4c. The prediction assessment described by the overall $K^{\text{enhancement}}$ strongly correlated with the survival time suggesting that animals with higher intratumoral uptake of the nanocarrier as imaged with mammography survived longer. While the k_1 and k_2 signal enhancement rate constants of the individual treatments positively correlated with the survival time (Pearson's $R^2=0.63$ and 0.72 respectively), the overall K provided the most reliable prediction (Pearson's $R^2=0.84$).

4. Discussion

Tumor chemotherapy is often iterative, alternating 'treatment' periods with intermittent assessment periods that are used to fine tune dosing, evaluate efficacy and consider alternative drugs or treatment regimens. Besides breast cancer tumor staging and hormonal status, unfortunately, the clinician typically has little information to track and customize chemotherapy for each tumor in a patient-specific manner [34]. The multifunctional capabilities of nanotherapeutics such as those described in this study circumvent this problem by facilitating clinically relevant, timely feedback

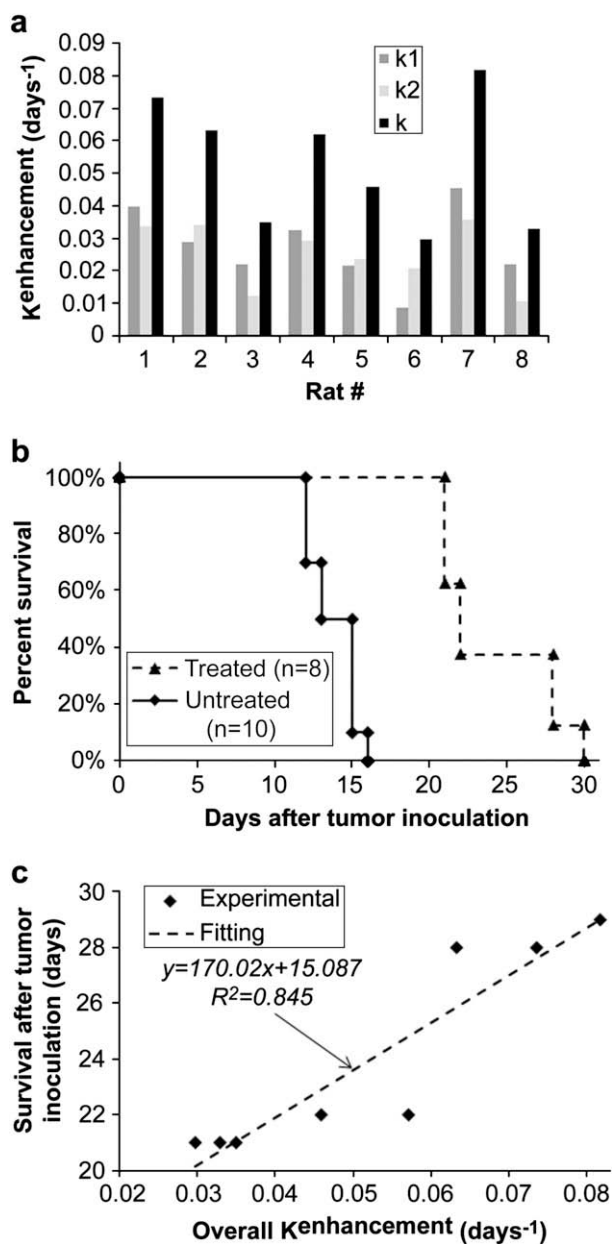


Fig. 4. Comparison of the imaging measurements to the survival time of animals injected once a week with the nanocarrier for a total of two cycles. (a) The tumor signal enhancement rate constants of the each treatments (k_1 and k_2) and the entire treatment (overall $K = k_1 + k_2$) displayed a broad variation; (b) The survival of the treated group ($n = 8$) was significantly prolonged when compared to an untreated group ($n = 10$, $p < 0.0006$; t -test, two-tailed); (c) The overall enhancement rate constant (K) of each animal strongly correlated to its survival time ($p < 0.001$; t -test, single-tailed).

on tumor dosing and distribution so that treatment decisions can be made in a patient-specific manner.

We previously reported a liposomal nanocarrier with prolonged blood circulation that encapsulated sufficient iodine to enable blood pool imaging [35,36]. While this contrast agent facilitates remarkable imaging of the heart and great vessels with minimal clearance of the contrast agent via the kidneys [35,36], its dose can be titrated to visualize the intratumoral, extravascular deposition of the agent without interference from a persistent intravascular signal. Therefore, a multifunctional nanocarrier and dosing regimen was designed based on the fact that 5–10% of a liposomal dose usually extravasates within 24 h in solid tumors [37,38] and 2.5 mg of (liposomal) iodine extravasated into tumors of about 1 cm in diameter can be detected reliably using mammography.

Even though the animals had tumors of similar size when the multifunctional agent was administered (Fig. 3d), the tumor X-ray absorption displayed a variation among the animals with the standard deviation representing 40% of the mean value (3 days post-injection; Fig. 3b) which strongly correlated with the amounts of drug deposited in the tumor (Fig. 3f). These data are consistent with clinical studies in which the biodistribution of radiolabeled liposomes was studied in cancer patients showing a considerable heterogeneity of the liposomal intratumoral deposition among different cancer types and among patients with the same tumor type [39]. Variation of the liposomal doxorubicin intratumoral deposition has also been observed in biopsy specimens of Kaposi's sarcoma lesions in clinical studies with the standard deviation ranging from 20 to 50% of the mean value [40]. Besides clinical studies, numerous studies with liposomal doxorubicin were conducted in invasive and well-vascularized xenograft mouse models including human breast cancer models (e.g. MDA-MB-435 and MCF-7 adenocarcinomas, BT474 ductal carcinoma [41,42]) and human ovarian cancer models (e.g. OVCAR3 and ES-2 ovarian carcinomas [43]). In all these studies, liposomes exhibited significant variation in intratumoral accumulation and antitumor effects. The variability in temporal and spatial accumulation of extravasated nanoparticles is attributed to variable degree of vascularization, blood flow, vessel permeability, cellularity, interstitial pressure, and the fraction of the extracellular space [44]. In addition to the different vascular permeability to nanoparticles of the same type tumors [23,26], the same tumor displays a vasculature with continuous spatial and temporal changes during growth, regression, and relapse [22].

Significantly, mammographic determination of variability of the intratumoral nanocarrier uptake provided an accurate prognosis of the therapeutic outcome. The tumor response represented by the tumor growth rate exhibited a variation consistent with previous studies using human breast tumor xenografts in nude mice treated with liposomal doxorubicin [41]. Although technically, the tumor leakiness can be probed using a contrast agent, and then therapeutic administered in a sequential basis, the aggressiveness of this tumor and fast changes in vascular permeability in space and time preclude this option rendering a multifunctional co-encapsulation approach as the desired approach for fast growing tumors. While our data indicate that imaging-based prediction for each treatment cycle is ideal in the MAT BIII animal model, we hypothesize one imaging-based prediction may be adequate to predict outcomes in less aggressive tumors with low proliferation rates.

While several different nanocarrier chemistries can be designed, one of the important advantages of the liposomal nanocarrier system is their high potential for clinical translation based on their long and successful history of encapsulating agents such as DXR (as in the product Doxil[®]) for clinical use. Thus, while more intricate nanoparticle systems may be novel from a materials science perspective, their potential for translation to clinical use is limited by the dearth of knowledge about their toxicity, biodistribution and in vivo fate, while liposomal nanoparticles are relatively well characterized and thus provide the potential for rapid translation to the clinic. Furthermore, liposomal DXR was the first nanotherapeutic to be approved for clinical use as the first line for treatment of AIDS-related Kaposi's Sarcoma and relapsed ovarian cancer [4]. There are currently 81 ongoing clinical trials in the US (www.ClinicalTrials.gov; accessed 5/29/2008), of liposomal DXR (Doxil[®] and various generic equivalence candidates) in a wide range of tumors including breast cancer which accounts for 23 active studies. Besides liposomal DXR, other liposomal formulations are under preclinical and clinical evaluation having payloads such as drugs (e.g. camptothecin analog, interleukin 2, cisplatin) and genes [6].

Such multifunctional nanocarriers are ideal agents for cancer therapy since imaging and therapy are provided within the same nanocarrier. Although drug levels in tumor tissues can be samples using microdialysis [45–48], non-invasive clinical methods have not yet been developed. PET imaging of radiolabeled nanotherapeutics [39] or MR imaging of nanocarriers co-loaded with a drug and paramagnetic contrast agents [9] can provide alternative solutions. Taking under consideration that mammography prevails as the only method of low cost mass screening of the general population for non-palpable breast cancer and the total X-ray dose required for such imaging is acceptable for clinical use, such prognosis would be quite practical. Though planar X-ray imaging-enabled prognosis in this study, we hypothesize that tomographic methods (e.g. CT) could provide equally good or even better prognosis since 3-dimensional information on extravasatory structures could be exploited to yield further insights into the susceptibility of the tumor to nanoparticle chemotherapy.

5. Conclusions

In this work, the fabrication of a multifunctional 100 nm scale nanocarrier containing a contrast agent for X-ray imaging and a chemotherapeutic for therapy is shown. We demonstrate that the multifunctionality of the nanocarrier enabled live monitoring and prediction of the outcome of breast cancer therapy using mammography. Such determination of the amount of chemotherapeutic reaching and remaining in the tumor during each treatment can potentially ensure an optimized, personalized therapy regimen and spare non-responders from the rigors of a chemotherapy regimen.

Acknowledgements

This work was supported in part by National Science Foundation Bioengineering and Environmental Systems 0401627 (RVB), Georgia Tech/Emory Center for Engineering Living Tissues an NSF ERC – EEC-9731643 (Nerem), the Nora L. Redman Fund (RVB), the Wallace H. Coulter Foundation (RVB), and the Georgia Cancer Coalition (RVB).

References

- Gradishar WJ, Tjulandin S, Davidson N, Shaw H, Desai N, Bhar P, et al. Phase III trial of nanoparticle albumin-bound paclitaxel compared with polyethylated castor oil-based paclitaxel in women with breast cancer. *J Clin Oncol* 2005 Nov 1;23(31):7794–803.
- Lasic DD. Doxorubicin in sterically stabilized liposomes. *Nature* 1996 Apr 11;380(6574):561–2.
- Yezhelyev MV, Gao X, Xing Y, Al-Hajj A, Nie S, O'Regan RM. Emerging use of nanoparticles in diagnosis and treatment of breast cancer. *Lancet Oncol* 2006 Aug;7(8):657–67.
- Lasic DD, Papahadjopoulos D. Liposomes revisited. *Science* 1995 Mar 3;267(5202):1275–6.
- Pope-Harman A, Cheng MM, Robertson F, Sakamoto J, Ferrari M. Biomedical nanotechnology for cancer. *Med Clin North Am* 2007 Sep;91(5):899–927.
- Ferrari M. Cancer nanotechnology: opportunities and challenges. *Nat Rev Cancer* 2005 Mar;5(3):161–71.
- Service RF. Materials and biology. Nanotechnology takes aim at cancer. *Science* 2005 Nov 18;310(5751):1132–4.
- Derfus AM, Chen AA, Min DH, Ruoslahti E, Bhatia SN. Targeted quantum dot conjugates for siRNA delivery. *Bioconjug Chem* 2007 Sep–Oct;18(5):1391–6.
- Viglianti BL, Abraham SA, Michelich CR, Yarmolenko PS, MacFall JR, Bally MB, et al. In vivo monitoring of tissue pharmacokinetics of liposome/drug using MRI: illustration of targeted delivery. *Magn Reson Med* 2004 Jun;51(6):1153–62.
- Saul JM, Annapragada AV, Bellamkonda RV. A dual-ligand approach for enhancing targeting selectivity of therapeutic nanocarriers. *J Controlled Release* 2006 Sep 12;114(3):277–87.
- Hong S, Leroueil PR, Majoros IJ, Orr BG, Baker Jr JR, Banaszak Holl MM. The binding avidity of a nanoparticle-based multivalent targeted drug delivery platform. *Chem Biol* 2007 Jan;14(1):107–15.
- van de Wiele P, Dierckx R, Scopinaro F, Waterhouse R, Annovazzi A, Kolindou A, et al. Nuclear medicine imaging for prediction or early assessment of response to chemotherapy in patients suffering from breast carcinoma. *Breast Cancer Res Treat* 2002 Apr;72(3):279–86.
- Koning GA, Krijger GC. Targeted multifunctional lipid-based nanocarriers for image-guided drug delivery. *Anticancer Agents Med Chem* 2007 Jul;7(4):425–40.
- Torchilin VP. Multifunctional nanocarriers. *Adv Drug Deliv Rev* 2006 Dec 1;58(14):1532–55.
- Mitra A, Nan A, Line BR, Ghandehari H. Nanocarriers for nuclear imaging and radiotherapy of cancer. *Curr Pharm Des* 2006;12(36):4729–49.
- Folkman J. Angiogenesis in cancer, vascular, rheumatoid and other disease. *Nat Med* 1995 Jan;1(1):27–31.
- Jain RK. Transport of molecules, particles, and cells in solid tumors. *Annu Rev Biomed Eng* 1999;1:241–63.
- Jain RK. Barriers to drug delivery in solid tumors. *Sci Am* 1994 Jul;271(1):58–65.
- Jain RK. Delivery of molecular and cellular medicine to solid tumors. *Adv Drug Deliv Rev* 2001 Mar 1;46(1–3):149–68.
- Maeda H, Wu J, Sawa T, Matsumura Y, Hori K. Tumor vascular permeability and the EPR effect in macromolecular therapeutics: a review. *J Controlled Release* 2000 Mar 1;65(1–2):271–84.
- Wolff AC. Liposomal anthracyclines and new treatment approaches for breast cancer. *Oncologist* 2003;8(Suppl. 2):25–30.
- Fukumura D, Jain RK. Tumor microenvironment abnormalities: causes, consequences, and strategies to normalize. *J Cell Biochem* 2007 Jul 1;101(4):937–49.
- Hobbs SK, Monsky WL, Yuan F, Roberts WG, Griffith L, Torchilin VP, et al. Regulation of transport pathways in tumor vessels: role of tumor type and microenvironment. *Proc Natl Acad Sci U S A* 1998 Apr 14;95(8):4607–12.
- Yuan F, Chen Y, Dellian M, Safabakhsh N, Ferrara N, Jain RK. Time-dependent vascular regression and permeability changes in established human tumor xenografts induced by an anti-vascular endothelial growth factor/vascular permeability factor antibody. *Proc Natl Acad Sci U S A* 1996 Dec 10;93(25):14765–70.
- Jain RK. Normalization of tumor vasculature: an emerging concept in anti-angiogenic therapy. *Science* 2005;307(5706):58–62.
- Fukumura D, Jain RK. Tumor microvasculature and microenvironment: targets for anti-angiogenesis and normalization. *Microvasc Res* 2007 May 18.
- Bolotin EM, Cohen R, Bar LK, Emanuel N, Ninio S, Lasic DD, et al. Ammonium sulfate gradients for efficient and stable remote loading of amphipathic weak bases into liposomes and ligandoliposomes. *J Liposome Res* 1994;4:455–79.
- Hubbell JH, Seltzer SM. Tables of X-ray mass attenuation coefficients and mass energy-absorption coefficients. Available from: <http://physics.nist.gov/PhysRefData/XrayMassCoef/cover.html>; 1996 [accessed 12.05.07].
- Sechopoulos I, Suryanarayanan S, Vedantham S, D'Orsi C, Karellas A. Computation of the glandular radiation dose in digital tomosynthesis of the breast. *Med Phys* 2007;34(1):221–32.
- Boone JM. Normalized glandular dose (Dgn) coefficients for arbitrary X-ray spectra in mammography: computer-fit values of Monte Carlo derived data. *Med Phys* 2002 May;29(5):869–75.
- Charrois GJ, Allen TM. Drug release rate influences the pharmacokinetics, biodistribution, therapeutic activity, and toxicity of pegylated liposomal doxorubicin formulations in murine breast cancer. *Biochim Biophys Acta* 2004;1663(1–2):167–77.
- Jabri KN, Wilson DL. Quantitative assessment of image quality enhancement due to unsharp-mask processing in X-ray fluoroscopy. *J Opt Soc Am A Opt Image Sci Vis* 2002 Jul;19(7):1297–307.
- Brown BW, Atkinson EN, Bartoszynski R, Thompson JR, Montague ED. Estimation of human tumor growth rate from distribution of response size at detection. *J Natl Cancer Inst* 1984 Jan;72(1):31–8.
- Tewari M, Krishnamurthy A, Shukla HS. Predictive markers of response to neoadjuvant chemotherapy in breast cancer. *Surg Oncol* 2008 May 6.
- Kao CY, Hoffman EA, Beck KC, Bellamkonda RV, Annapragada AV. Long-residence-time nano-scale liposomal iohexol for X-ray – based blood pool imaging. *Acad Radiol* 2003;10:475–83.
- Mukundan S, Ghaghada KB, Badea CT, Kao CY, Hedlund LW, Provenzale JM, et al. A liposomal nanoscale contrast agent for preclinical CT in mice. *AJR Am J Roentgenol* 2006;186:300–7.
- Gabizon A, Martin F. Polyethylene glycol-coated (pegylated) liposomal doxorubicin. Rationale for use in solid tumours. *Drugs* 1997;54(Suppl. 4):15–21.
- Harrington KJ. Liposomal cancer chemotherapy: current clinical applications and future prospects. *Expert Opin Investig Drugs* 2001 Jun;10(6):1045–61.
- Harrington KJ, Mohammadtaghi S, Uster PS, Glass D, Peters AM, Vile RG, et al. Effective targeting of solid tumors in patients with locally advanced cancers by radiolabeled pegylated liposomes. *Clin Cancer Res* 2001 Feb;7(2):243–54.
- Northfelt DW, Martin FJ, Working P, Volberding PA, Russell J, Newman M, et al. Doxorubicin encapsulated in liposomes containing surface-bound polyethylene glycol: pharmacokinetics, tumor localization, and safety in patients with AIDS-related Kaposi's sarcoma. *J Clin Pharmacol* 1996 Jan;36(1):55–63.
- Park JW, Hong K, Kirpotin DB, Colbern G, Shalaby R, Baselga J, et al. Anti-HER2 immunoliposomes: enhanced efficacy attributable to targeted delivery. *Clin Cancer Res* 2002 Apr;8(4):1172–81.
- Kirpotin DB, Drummond DC, Shao Y, Shalaby MR, Hong K, Nielsen UB, et al. Antibody targeting of long-circulating lipidic nanoparticles does not increase tumor localization but does increase internalization in animal models. *Cancer Res* 2006;66:6732–40.

- [43] Saucier JM, Yu J, Gaikwad A, Coleman RL, Wolf JK, Smith JA. Determination of the optimal combination chemotherapy regimen for treatment of platinum-resistant ovarian cancer in nude mouse model. *J Oncol Pharm Pract* 2007 Mar;13(1):39–45.
- [44] Nunes FL, Schiabel H, Benatti RH. Contrast enhancement in dense breast images using the modulation transfer function. *Med Phys* 2002 Dec;29(12):2925–36.
- [45] Muller M, Mader RM, Steiner B, Steger GG, Jansen B, Gnant M, et al. 5-fluorouracil kinetics in the interstitial tumor space: clinical response in breast cancer patients. *Cancer Res* 1997 Jul 1;57(13):2598–601.
- [46] Blochl-Daum B, Muller M, Meisinger V, Eichler HG, Fassolt A, Pehamberger H. Measurement of extracellular fluid carboplatin kinetics in melanoma metastases with microdialysis. *Br J Cancer* 1996 Apr;73(7):920–4.
- [47] Palsmeier RK, Lunte CE. Microdialysis sampling in tumor and muscle: study of the disposition of 3-amino-1,2,4-benzotriazine-1,4-di-N-oxide (SR 4233). *Life Sci* 1994;55(10):815–25.
- [48] Muller M, Schmid R, Georgopoulos A, Buxbaum A, Wasicek C, Eichler HG. Application of microdialysis to clinical pharmacokinetics in humans. *Clin Pharmacol Ther* 1995 Apr;57(4):371–80.